AI-Driven Personalized Physical Education and Improvement of Key Physical Fitness Characteristics

Xiaoyan Hu, Minghuan Tang

School of Physical Education, Beibu Gulf University, Qinzhou 535011, Guangxi, China

Corresponding author: Minghuan Tang (e-mail: tmh6366@163.com)

ABSTRACT This study proposes an AI-driven adaptive framework for personalized physical training based on multimodal sensing, real-time signal fusion, and hierarchical decision optimization. A heterogeneous sensing architecture integrating smartphone vision sensors and wearable physiological devices is developed to acquire synchronized kinematic and physiological information. A multimodal state perception layer combines motion-derived features, physiological measurements, and temporal synchronization mechanisms to generate unified state representations for continuous individual monitoring. To characterize long-term behavioral evolution, an incremental clustering strategy is introduced to dynamically update user profiles, while a weighted knowledge graph establishes quantitative relationships between physical fitness attributes and training actions. Furthermore, a hierarchical reinforcement learning framework is constructed, where a deep Q-network regulates training-load allocation and a proximal policy optimization network generates adaptive action sequences. An edge-deployable feedback module incorporating real-time motion analysis and augmented-reality-assisted correction is integrated to form a closed-loop sensing and control architecture. Experimental evaluation involving 1,286 students over a 12-week intervention period demonstrates an average improvement of 12.3 points in key physical fitness indicators, while the individual adaptability index increases from 0.732 to 0.901. The proposed framework establishes a unified methodology for multimodal signal acquisition, adaptive information processing, and closed-loop feedback optimization, providing an engineering-oriented solution for large-scale intelligent sensing and human-centered monitoring systems.

INDEX TERMS multimodal sensing, signal fusion, reinforcement learning, closed-loop feedback

I. INTRODUCTION

ARTIFICIAL intelligence technology has shown significant potential in areas such as motion posture recognition, load monitoring, and feedback intervention, providing a new path for realizing the vision of "teaching according to aptitude" in physical education [1,2]. However, the current AI-enabled physical education still faces significant bottlenecks: most systems rely on static rules or fixed model architectures, making it difficult to dynamically capture the multidimensional heterogeneous characteristics of students in terms of physiological development, motor ability, psychological state, and environmental adaptation [3,4]. Especially in the long-term teaching process, students' physical fitness development is nonlinear, time-varying, and individual-specific, leading to the rapid decay of effective interventions in generalized models over time, and even causing training overload or decreased motivation, which seriously restricts the accurate improvement of key physical fitness characteristics [5]. How to construct an adaptive AI model that can perceive individual status in real time and dynamically adjust teaching strategies has become the core challenge for personalized physical education from concept to practice.

Many studies have explored and contributed to the personalization of physical education and the improvement of key physical fitness. Garcia-Hermoso A has been tracking the physical development trajectory of adolescents for a long time. By analyzing physical activity and sports participation, he explored the tracking of physical activity at different stages [6]. Wei L went a step further and used artificial intelligence to classify and analyze activities [7]. Li S et al. proposed a fuzzy evaluation model of college physical education teaching methods based on artificial intelligence, which can effectively improve teaching quality and students' physical fitness [8]. Cudicio A explored the application of artificial intelligence in personalized physical education, believing that personalized teaching is very important in the school environment and can help teachers customize courses and propose sustainable teaching methods based on the differences of students [9]. Yu X I N believes that artificial intelligence has a positive impact on adolescent physical education, which can bring about innovation in teaching methods and optimize students' extracurricular exercise [10]. The above studies indicate that artificial intelligence has a good effect on both the teaching quality of teachers and the personalized learning and physical fitness improvement of students.

In response to the challenges of personalized physical education and key physical fitness improvement, scholars at home and abroad have carried out a series of algorithm explorations. Cao M improved the Apriori algorithm to improve the efficiency and accuracy of data association rule mining in physical education, which has contributed to meeting students' personalized sports needs, but did not consider the multi-movement switching scenario in real physical education classes [11]; Li G used multimedia learning platforms and datadriven teaching to improve physical education, and achieved personalization by integrating data, but its update mechanism resulted in a long update cycle and difficulty in real-time response [12]; Tian Y predicted students' learning outcomes based on big data analysis, integrated and analyzed clear data and fuzzy data to provide useful information, guide the improvement of courses and teaching strategies, and provide personalized teaching methods [13]; Mou C constructed a sports intelligent teaching system based on data mining and virtual simulation technology, which helps to formulate personalized training strategies and skills [14]; deep learning has also been used in physical education, and personalized learning effects can be achieved by tracking and analyzing students' physical fitness data [15,16]. The fuzzy C-means algorithm has also been used for the personalization of physical education, and can recommend suitable learning resources for different learners [17,18]. Existing research has widely applied various intelligent algorithms to personalize physical education and improve physical fitness. However, they lack the ability to continuously perceive and adapt to students' dynamic characteristics, making it difficult to achieve long-term stable personalized intervention. Therefore, constructing an AI model capable of real-time perception and dynamic adjustment is crucial for achieving continuous improvement in key physical fitness levels.

This paper aims to construct a dynamically adaptive personalized physical education teaching model. First, it uses heterogeneous sensors to simultaneously collect students' kinematic and physiological signals, constructing a real-time state perception layer. Then, it designs an incremental clustering mechanism to dynamically depict the evolution trajectory of students' physical fitness characteristics. This builds a directed knowledge graph with expert knowledge that quantifies the contribution of 127 standardised physical movements to the six primary attributes of physical fitness. This knowledge graph will act as a foundational lookup table for the reinforcement learning agent. The agent will use the knowledge graph to target the correct productivity improvements by finding and ranking the most efficient, pre-validated movements to be included in the individualised training order; thus, using expert knowledge as the basis for algorithmic decisions. Finally, relying on a reinforcement learning framework that coordinates the outer and inner loops, it generates and adjusts personalized training plans in real time, supplemented by AR (Augmented Reality) visualization feedback and a teacher collaborative intervention interface. By integrating data collection and individual modeling with the precision of automated design, this research achieves a seamless transition from knowledge guidance to dynamic decision-making, optimizing students' physical fitness and safety through a technical paradigm akin to the high-quality synthesis of intelligent fiber systems.

II. AI-DRIVEN PERSONALIZED PHYSICAL EDUCATION TEACHING MODEL

A. CONSTRUCTION OF MULTIMODAL STUDENT STATE AWARENESS LAYER

The system employs a heterogeneous sensor collaborative deployment scheme, using a smartphone and a smart bracelet to form a dual-source synchronous acquisition architecture. The smartphone camera's / Intrinsic Parameter Calibration uses the checkerboard method of Offline Calibration. To perform Extrinsic Calibration for the Initial Alignment of the camera and inertial measurement unit coordinate systems, the student will wear the bracelet on his or her NON-dominant wrist while standing in a fixed position, or upright inside the static camera's field of view, for purposes of establishing a baseline transformation for future locomotive activities such as the 1000m run. The smartphone camera will not be mounted on a tripod during physical education sessions, but will be remotely operated by a teaching assistant or placed at an elevated fixed location. The smartphone camera will be aimed to have a wide field of view in order to capture the designated exercise area, such as a section of a running track or a gym. The video footage of the student running will first be recorded while the student is moving through the smartphone camera's field of view, therefore kinematic analysis will take place with the system processing kinematic data discontinuously, but repeatedly. The primary way that kinematic information will be captured continuously while covering a full session will be through the inertial data collected from the smart bracelet and will have periodic validation through the video footage to confirm form and full body posture. The architecture of the multimodal student state perception layer is shown in Figure 1.

Figure 1 shows the architecture of the multimodal student state perception layer. After the data is collected, the video stream is processed by MediaPipe Pose to infer the coordinates of 33 3D human joints in real time: $\mathbf{p}_j^t = (x_j^t, y_j^t, z_j^t) \in \mathbb{R}^3$, where $j \in \{0, 1, \ldots, 32\}$ represents the joint index (e.g., $j = 25$ for the left knee), and t is the frame number [19]. The depth information z_j^t is recovered by monocular scale normalization, and the coordinate system is aligned with the midpoint of the hip joint $\mathbf{c}_{\text{hip}}^t = \frac{1}{2}(\mathbf{p}_{23}^t + \mathbf{p}_{24}^t)$

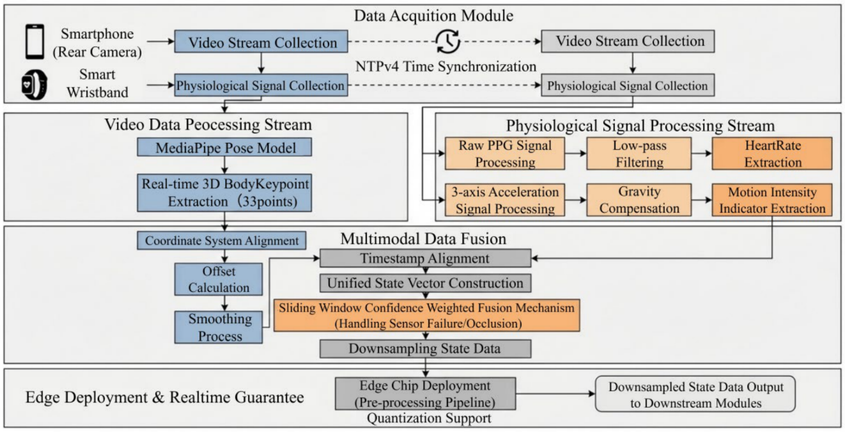

FIGURE 1. Architecture Diagram of the Multimodal Student State Awareness Layer

as the origin to eliminate translational degrees of freedom [20,21].

The knee joint angular velocity ω^t_{knee} is estimatedby the differential cross product of the joint vectors in three consec utive frames: let $\mathbf{v}^t_1 = \mathbf{p}^t_{23} - \mathbf{p}^t_{25}$ (hip-knee) and $\mathbf{v}^t_2 = \mathbf{p}^t_{27} - \mathbf{p}^t_{25}$ (ankle-knee), then the instantaneous angular veloc ity magnitude of the knee joint is:

$$\omega^t_{\text{knee}} = \frac{1}{\Delta t}\left\| \frac{\mathbf{v}^t_1 \times \mathbf{v}^t_2}{\|\mathbf{v}^t_1\| \cdot \|\mathbf{v}^t_2\|} - \frac{\mathbf{v}^{t-1}_1 \times \mathbf{v}^{t-1}_2}{\|\mathbf{v}^{t-1}_1\| \cdot \|\mathbf{v}^{t-1}_2\|} \right\| \quad (1)$$

In equation (1), $\Delta t = 1/30$s represents the frame interval; this construction avoids Euler angle singularity and exhibits normalization robustness to changes in limb scale. The horizontal offset of the center of gravity δ^t_{COM} is defined as the projected distance between the midpoint of the ankle joint and the midpoint of the hip joint on the X-axis of the image plane:

$$\delta^t_{\text{COM}} = \left| \frac{x^t_{27} + x^t_{28}}{2} - \frac{x^t_{23} + x^t_{24}}{2} \right| \quad (2)$$

This index quantifies dynamic balance ability and is sensitive to the stability of actions such as jumping landing and changing direction. To suppress high-frequency jitter, a five-point Savitzky-Golay smoothing (window length 5, quadratic polynomial fitting) is applied to δ^t_{COM}. The physiological signal processing chain consists of three stages: the original PPG (Photoplethysmography) signal is filtered by a 5th-order Butterworth lowpass filter (cutoff frequency $f_c = 0.5$Hz) to suppress motion artifacts [22,23]; the heart rate HR^t is obtained by adaptive peak detection (the threshold is dynamically updated to 70% of the mean local R-wave amplitude); the triaxial acceleration $\mathbf{a}^t = (a^t_x, a^t_y, a^t_z)$ is compensated for by gravity components (using complementary filtering to fuse the gyroscope angular velocity integral) and the vector amplitude $VM^t = \sqrt{(a^t_x)^2 + (a^t_y)^2 + (a^t_z)^2 - 1^2}$ is extracted as a proxy variable for local motion intensity. Initial synchronization of the smartwatch and smartphone will occur prior to the start of each data collection session using the NTPv4 protocol. However, practical considerations such as differences in latency during Bluetooth communication, the stability of internal clock oscillators between the smartwatch and smartphone (with the smartwatch being a low power device), and the mobile processor being intermittently loaded can lead to variable and non-constant accumulating clock drift during the session. All modal data are aligned with a unified timestamp: the video frame timestamp t_v and the wristband sampling timestamp t_s are mapped by least squares linear regression $t_s = \alpha t_v + \beta$, and after synchronization, a state vector $\mathbf{s}_t = [\omega^t_{\text{knee}}, \delta^t_{\text{COM}}, HR^t, VM^t]^\top \in \mathbb{R}^4$ is constructed and output to the downstream module at a 10 Hz downsampling rate. To cope with occlusion and sensor failure, a sliding window confidence weighted fusion mechanism is designed. If the MediaPipe key point detection confidence $\gamma^t_j < 0.6$ lasts for more than 5 frames, the kinematic features ω^t_{knee} and δ^t_{COM} are not computed from the corrupted visual data. Instead, the system switches to a conservative state estimation mode. In this mode, the most recent valid estimates of ω^t_{knee} and δ^t_{COM} from the preceding 2-second window are held constant and used as imputed values for the duration of the occlusion event. This imputation strategy, coupled with the continued use of the real-time physiological signals HR^t and VM^t, maintains the continuity of the state vector $\mathbf{s}_t$ without injecting the physically implausible signal of zero angular velocity and zero center-of-mass offset. The system reverts to standard computation upon the restoration of sufficient keypoint detection confidence.

B. DYNAMIC STUDENT PROFILE UPDATE MECHANISM BASED ON INCREMENTAL CLUSTERING

The initial profile was constructed based on six indicators of the physical fitness test for college entrance: standing long jump, $4 \times 15\text{m}$ shuttle run, 1000m/800m run, pull-ups/sit-ups, sit-and-reach, and 30-second double unders. The original data vector $\mathbf{x}^{(0)}_i = [x_1, x_2, x_3, x_4, x_5, x_6]^\top$ was normalized by Z-score and then input into principal component analysis (PCA). The top three principal components with a cumulative variance contribution rate

$\geq$92% were retained, resulting in the dimension-reduced representation $\mathbf{z}_i^{(0)} = W_3^\top(\mathbf{x}_i^{(0)} - \boldsymbol{\mu})$, where $\boldsymbol{\mu}$ is the mean vector and W_3 is the projection matrix composed of the top three feature vectors. This dimension reduction effectively alleviates the clustering bias caused by the difference in the scale of the indicators. The first principal component showed strong positive loadings on the standing long jump and the 4×15m shuttle run, representing a composite dimension of lower-body power and speed-agility. The second principal component was dominated by positive loadings on the 1000m/800m run and pull-ups/sit-ups, capturing an endurance and muscular endurance dimension. The third principal component exhibited a high positive loading on the sit-and-reach test, associated primarily with flexibility. The 30 second double under contributions were spread out across both the first and second component contributions, allowing for a basis for interpreting the dimensions that provided a framework for naming the clusters from the reduced form. With $\{\mathbf{z}_i^{(0)}\}_{i=1}^N$ as input, K-means++ initialization was performed [24], the initial number of clusters $k^{(0)}$ was set, and the initial cluster center set $C^{(0)}$ was obtained. The clustering results were validated using silhouette coefficients. Each cluster corresponds to a typical physical fitness type: Type-A (power-explosive dominance), Type-B (flexibility-coordination dominance), Type-C (speed-agility dominance), Type-D (endurance dominance), and Type-E (balanced development) [25,26].

The system employs an incremental update mechanism: at the end of each week, the individual state summary vector $\mathbf{z}_i^{(w)} \in \mathbb{R}^3$ of all valid courses for that week is summarized. This vector is generated by time-series pooling from the $\mathbf{s}_t$ of the three courses for that week. For each course, the mean joint angular velocity and the standard deviation of the center of gravity offset are calculated, and then mapped isomorphically to the initial PCA [27,28]. For a new sample $\mathbf{z}_i^{(w)}$, the Euclidean distance $d_j = \|\mathbf{z}_i^{(w)} - \mathbf{c}_j^{(w-1)}\|_2$ to the center of each existing cluster is calculated, and the minimum distance $d_{\min} = \min_j d_j$ is taken. A dynamic threshold is defined:

$$\tau^{(w)} = 0.8 \times \frac{1}{k^{(w-1)}} \sum_{j=1}^{k^{(w-1)}} \frac{1}{|S_j^{(w-1)}|} \sum_{\mathbf{z} \in S_j^{(w-1)}} \|\mathbf{z} - \mathbf{c}_j^{(w-1)}\|_2 \tag{3}$$

In equation (3), $S_j^{(w-1)}$ is the sample set of the j-th cluster in week $w-1$, and $|S_j^{(w-1)}|$ is its cardinality; $\tau^{(w)}$ represents the average intra-cluster dispersion of the current clustering structure. If $d_{\min} > \tau^{(w)}$, the sample is determined to significantly deviate from the existing pattern, triggering cluster expansion: a new center $\mathbf{c}_{k^{(w-1)}+1}^{(w)} \leftarrow \mathbf{z}_i^{(w)}$ is added, and a single round of K-means re-clustering is performed with all current samples. The student dynamic type identifier $T_i^{(w)} = \arg\min_j \|\mathbf{z}_i^{(w)} - \mathbf{c}_j^{(w)}\|_2$ is used as its main label for the current week's profile; to characterize cross-cluster transition, a soft membership label is introduced:

$$\begin{aligned} \alpha_{ij}^{(w)} &= \frac{\exp\left(-\|\mathbf{z}_i^{(w)} - \mathbf{c}_j^{(w)}\|_2^2/\sigma^2\right)}{\sum_{l=1}^{k^{(w)}} \exp\left(-\|\mathbf{z}_i^{(w)} - \mathbf{c}_l^{(w)}\|_2^2/\sigma^2\right)}, \\ \sigma &= \frac{1}{k^{(w)}} \sum_{j=1}^{k^{(w)}} \|\mathbf{c}_j^{(w)} - \bar{\mathbf{c}}^{(w)}\|_2 \end{aligned} \tag{4}$$

In equation (4), $\bar{\mathbf{c}}^{(w)}$ is the mean of all current cluster centers; $\alpha_{ij}^{(w)}$ is used for weighting action weights in the downstream plan generator to avoid abrupt changes in the training scheme caused by hard switching.

C. CONSTRUCTION OF KEY PHYSICAL FITNESS-ACTION MAPPING KNOWLEDGE GRAPH

The knowledge graph is defined as a directed weighted graph $G = (V, E)$, where the node set is $V = V_{\text{PF}} \cup V_{\text{EX}}$. Here $V_{\text{PF}} = \{v_1, \ldots, v_6\}$ are six types of key physical fitness feature nodes: v_1 =ExplosivePower, v_2 =Agility, v_3 =Endurance, v_4 =CoreStability, v_5 =Flexibility, and v_6 =Coordination. $V_{\text{EX}} = \{u_1, \ldots, u_{127}\}$ are 127 standardized sports action nodes, such as u_{42} =LungeJump and u_{89} =PlankWithShoulderTap.

The edge set $E \subseteq V_{\text{PF}} \times V_{\text{EX}}$ represents the contribution relationship between physical fitness and action. Each edge $(v_p, u_e) \in E$ is associated with a weight $w_{pe} \in [0, 1]$, which represents the relative effectiveness of action u_e in improving physical fitness v_p. The weights were obtained using the improved Delphi method: three experts were invited to score independently using a Likert 5-point scale: 1 = "almost no contribution", 2 = "weak contribution", 3 = "moderate contribution", 4 = "significant contribution", 5 = "core contribution" [29,30]. A structured workshop was organized for items with significant disagreements in the first round, providing action activation spectra and summaries of kinematic parameters for the second round of scoring. Finally, the mean of the three scores, $\bar{r}_{pe}^{(2)}$, was taken and normalized to the unit interval by Min-Max.

$$w_{pe} = \frac{\bar{r}_{pe}^{(2)} - \min_{p',e'} \bar{r}_{p'e'}^{(2)}}{\max_{p',e'} \bar{r}_{p'e'}^{(2)} - \min_{p',e'} \bar{r}_{p'e'}^{(2)}} \tag{5}$$

After normalization, the weight distribution satisfies $\sum_{e=1}^{127} w_{pe} = 127$ (the total score of each physical fitness dimension is conserved), ensuring cross-physical fitness comparability; the Kendall coordination coefficient $W = 0.78$, indicating a high degree of expert consensus.

The graph is imported into Neo4j using the attribute graph model, and the edge attributes include w_{pe} and confidence level c_{pe}.

To support real-time teaching decisions, a two-level index is constructed. Physical energy-oriented index: For any physical energy v_p, pre-calculate its contribution ranking list $L_p = \arg\,\text{topk}_e(w_{pe})$, $k = 20$; Composite query interface:

input the target physical energy vector $\mathbf{q} = [q_1, \ldots, q_6]^\top$, $q_p \in [0,1]$, $\sum_p q_p = 1$, which are output by the outer loop strategy, and the system calculates the comprehensive action score:

$$s_e = \sum_{p=1}^{6} q_p \cdot w_{pe} \cdot c_{pe} \tag{6}$$

And returns $\arg\,\mathrm{top3}_e(s_e)$ and the corresponding (s_e, w_{pe}, c_{pe}) triplet; this weighted fusion mechanism allows high-confidence actions to be selected first and avoids interference from low-consensus actions.

D. DOUBLE-LOOP REINFORCEMENT LEARNING FRAMEWORK

This module adopts a hierarchical timing abstract architecture. The outer loop regulates the training load level at a weekly granularity, and the inner loop generates specific action sequences in units of single lessons. The two are coupled through the state-action interface.

The periodic control of the outer loop is instantiated as a deep Q network (DQN, Deep Q Network), and its state input is [31,32]:

$$s_t^{\text{outer}} = [\Delta EP_{t-1}, \Delta AG_{t-1}, FI_{t-1}]^\top \in \mathbb{R}^3 \tag{7}$$

In equation (7), $\Delta EP_{t-1} = EP_t - EP_{t-1}$ is the weekly increment of explosive power, ΔAG_{t-1} is similarly defined as the weekly increment of Agility, $FI_{t-1} = \frac{1}{3}\sum_{i=t-3}^{t-1} \mathrm{TRIMP}_i / \overline{\mathrm{TRIMP}}_{\mathrm{norm}}$ is the fatigue index ($\overline{\mathrm{TRIMP}}_{\mathrm{norm}}$ is the TRIMP of students in the same cluster in the same period (TRAining IMPulse) mean); the action space $A^{\text{outer}} = \{a_1, a_2, a_3\}$ corresponds to the load level and is mapped to the knowledge graph query weight vector $\mathbf{q}^{(a)}$. The reward function is designed as

$$r_t^{\text{outer}} = 0.7 \cdot \mathrm{sign}(\Delta S_t) + 0.3 \cdot m_t \tag{8}$$

In equation (8), $\Delta S_t = S_t - S_{t-1}$, $S_t = \sum_{p=1}^{6} w_p \cdot z_{p,t}$ is the weighted physical fitness comprehensive score, w_p is the weight, $z_{p,t}$ is the Z-score, $\mathrm{sign}(\cdot)$ ensures directional incentives; $m_t \in [0,1]$ is the student self-assessment motivation scale for the day to suppress the risk of overload. DQN uses 3-layer MLP (Multilayer Perceptron), with a target network update cycle of 200 steps; the experience replay pool capacity is 1000, and the priority sampling ratio is 0.6.

The class control of the inner loop is based on the $\mathbf{q}(a_t^{\text{outer}})$ output by the outer loop, calling the interface to obtain the Top-5 candidate action set $U_t = \{u_{t,1}, \ldots, u_{t,5}\}$; the state s_t^{inner} is composed of the real-time perception layer output splicing: for the current action window, the hip, knee, and ankle joint angle sequence $\theta_t \in \mathbb{R}^{3\times 32}$ and the heart rate sliding mean $\overline{HR}_t$ are extracted, and encoded into a 64-dimensional feature vector by 1D-CNN (1D Convolutional Neural Network). The action selection is output by the proximal policy optimization policy network $\pi_\theta(a \mid s)$, and its loss function is:

$$\begin{aligned} L^{\text{PPO}} &= \mathbb{E}_t[\min(\rho_t(\theta)A_t, \mathrm{clip}(\rho_t(\theta), 1-\epsilon, 1+\epsilon)A_t)] \\ &\quad - c_1 \mathbb{E}_t\left[(V_\phi(s_t) - R_t)^2\right] \end{aligned} \tag{9}$$

In equation (9), $\rho_t(\theta) = \frac{\pi_\theta(a_t|s_t)}{\pi_{\theta_{\text{old}}}(a_t|s_t)}$ is the importance sampling ratio, A_t is the GAE (Generalized advantage estimation) advantage estimate, $\epsilon = 0.2$ is the clipping threshold, $c_1 = 0.5$ is the value function loss coefficient, and V_ϕ is the state value function network. In order to enforce action diversity, the three consecutive action embedding vectors $\mathbf{e}_{t-2}$, $\mathbf{e}_{t-1}$, $\mathbf{e}_t$ (mapped by the action ID through the embedding layer) are constrained to satisfy $\frac{1}{3}\sum_{i<j} \frac{\mathbf{e}_i^\top \mathbf{e}_j}{\|\mathbf{e}_i\|\|\mathbf{e}_j\|} < 0.6$; if violated, a penalty term $\lambda_{\text{div}} \cdot \max(0, \mathrm{sim} - 0.6)$ can be added when the PPO gradient is updated. The loss curve is shown in Figure 2.

As can be seen in Figure 2, the loss value continues to decrease with the increase of training rounds, indicating that this loss function works well. In the dual-loop collaboration mechanism, the outer loop updates the load level every 72 lessons, and the inner loop generates an outer loop status correction signal at the end of each lesson based on the deviation between the actual TRIMP and the planned TRIMP. If the deviation between the actual TRIMP and the planned TRIMP is greater than 0.25 for two consecutive times, the outer loop redecision will be triggered in advance.

E. REAL-TIME ACTION FEEDBACK AND ERROR CORRECTION MODULE

This module implements millisecond-level closed-loop feedback of action quality, including four cascade links: start detection, trajectory alignment, deviation quantification, and augmented reality prompts. The real-time action feedback and error correction process is shown in Figure 3.

Action start detection uses the lightweight YOLOv5s (You Only Look Once v5s) model, which is deployed on the terminal to detect human body bounding boxes and key points in real time [33,34]; the start frame determination conditions are logical AND: (1) The vertical speed of the left/right hip joint is greater than 0.3 meters per second; (2) The mean coordinates of both wrist joints are lower than the midpoint of the lumbar spine.

Action trajectory alignment takes the starting frame as t_0, and intercepts the joint point sequence of the subsequent 20 frames; calculates the sagittal plane projection joint angle for the hip, knee, and ankle: $\phi_j^t = \arccos\left(\frac{(\mathbf{p}_{\text{prox}}^t - \mathbf{p}_j^t)\cdot(\mathbf{p}_{\text{dist}}^t - \mathbf{p}_j^t)}{\|\mathbf{p}_{\text{prox}}^t - \mathbf{p}_j^t\| \cdot \|\mathbf{p}_{\text{dist}}^t - \mathbf{p}_j^t\|}\right)$, where $\mathbf{p}_{\text{prox}}^t$ and $\mathbf{p}_{\text{dist}}^t$ are the coordinates of adjacent proximal/distal joint points; the angle sequence matrix Φ_{stu} is obtained. The standard template Φ_{std} is generated per movement from a normative database. This database contains motion capture sequences of the same action performed correctly by 30 individuals from the target demographic of junior high school students, with balanced representation across sexes and the previously identified physical fitness clusters. The sequences are time-aligned using dynamic time warping, and the mean trajec-

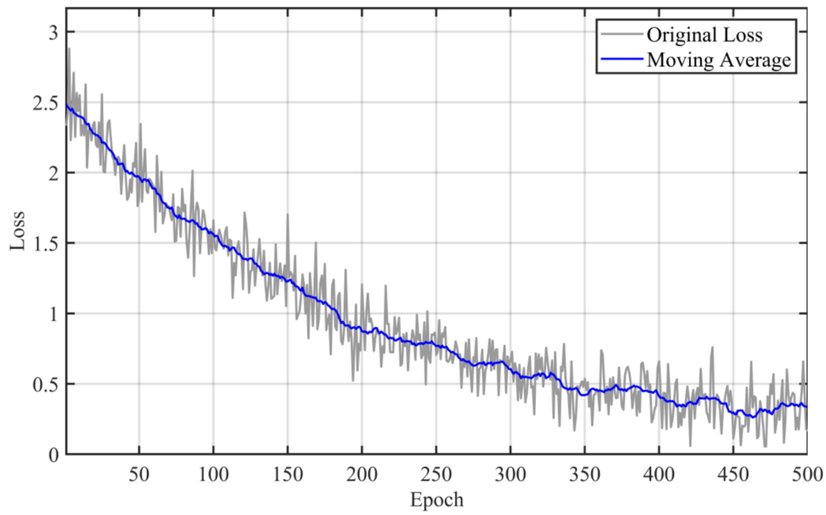

FIGURE 2. PPO Strategy Network Loss Curve

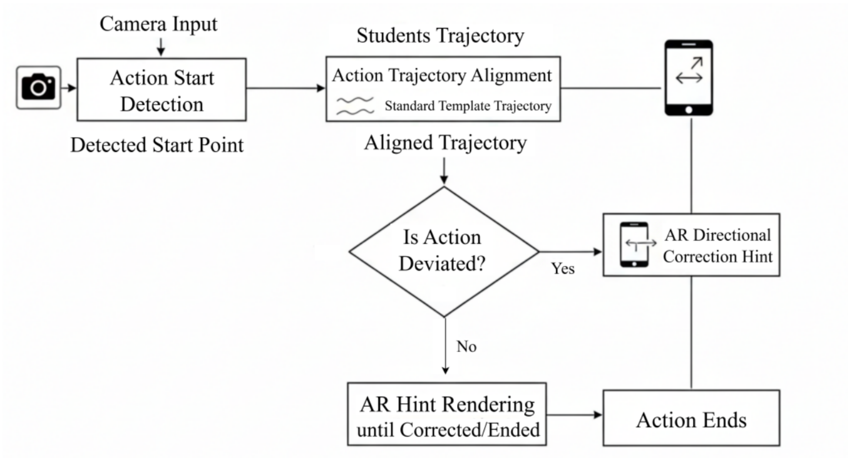

FIGURE 3. Real-time Action Feedback and Error Correction Flow Chart

tory across this demographically matched sample defines Φ_{std}. The reference parameters μ_{ref} and σ_{ref} used for Z-score normalization in the deviation calculation are also derived from this specific population database, ensuring age-appropriate and physically comparable kinematic benchmarks. Student trajectory alignment is solved by solving:

$$\pi^* = \arg\min_{\pi\in\Pi} \sum_{k=1}^{K} \|\Phi_{\text{stu}}(:,\pi_1(k)) - \Phi_{\text{std}}(:,\pi_2(k))\|_2^2 \quad (10)$$

In equation (10), Π is the set of all legal time warp paths, $\pi = (\pi_1, \pi_2)$ is the two-sequence index mapping, and FastDTW is used to accelerate the calculation.

The deviation determination is based on the aligned back angle sequence to calculate the DTW (Dynamic Time Warping) distance $d_{\text{DTW}} = \text{DTW}(\Phi_{\text{stu}}, \Phi_{\text{std}})$; in order to eliminate the dimensional difference between actions, Z-score standardization is introduced:

$$d_{\text{norm}} = \frac{d_{\text{DTW}} - \mu_{\text{ref}}}{\sigma_{\text{ref}}} \quad (11)$$

In equation (11), μ_{ref} and σ_{ref} are the d_{DTW} mean and standard deviation of 100 normative execution samples of the same action type and classmate portrait cluster; if $d_{\text{norm}} > 0.15$, the action is judged to be inaccurate. Further decompose d_{DTW} into joint components d_{hip}, d_{knee}, and d_{ankle} (weighted proportions of independent DTW distances based on the three-joint angle sequence) to locate the main source of deviation. AR prompt rendering uses ARCore to implement plane detection and attitude estimation; when $d_{\text{norm}} > 0.15$, a 3D arrow is superimposed on the mobile phone screen. When the absolute value of the yaw angle $\psi = \arctan 2(d_y, d_x) > 15°$, the arrow is set to red, otherwise it is yellow. The prompt lasts until the current action ends.

F. TEACHER COLLABORATIVE INTERVENTION INTERFACE DESIGN

This module implements precise intervention focusing on students with learning stagnation. The system automatically performs stagnation detection every Monday at 2:00 am. If the weighted physical fitness comprehensive score St meets the following requirements for two consecutive weeks:

$$\Delta S_{t-1} = S_{t-1} - S_{t-2} < \delta_{\text{th}}, \quad \Delta S_t = S_t - S_{t-1} < \delta_{\text{th}} \tag{12}$$

The student is then marked for entry into the intervention queue. The threshold δ_{th} is set based on the standard deviation of the measurement error during the baseline period to ensure that only true stagnation is captured. For each student, the system automatically generates a structured intervention package, which contains three parts:

(1) Deviation action video clips: Retrieve the DTW normalized distance d_{norm} maximum action sample in the past 14 days, intercept the video window centered on the starting frame, and superimpose error correction arrows and joint angle real-time curves;

(2) Diagnosis report of physical fitness shortcomings: Calculate the Z-score increment of 6 physical fitness items, and sort the minimum three items; combined with the dynamic portrait, call the cluster-specific reference value and output the shortcomings index;

(3) Intervention strategy set, generated by predefined decision trees. The depth of the decision tree is 4, and the remaining strategies are jointly screened and generated based on the knowledge graph.

After the intervention package is encrypted, it is pushed to the bound teacher APP [35] through Firebase cloud messages. The push fields include: student ID, stagnation weeks, hash verification code, and deadline processing time limit. After parsing, the teacher-side APP presents an interactive interface: the video can be played frame by frame and deviation points are marked; policy items support "adopt/modify/reject", and modifications need to be filled in with the basis; after the teacher confirms, the update instructions are synchronized to the student-side training plan generator, covering the subsequent three lesson action sequences.

III. EXPERIMENT AND VERIFICATION

A. EXPERIMENTAL DESIGN

This study uses schools as the randomization unit to avoid cross contamination. Eight public junior high schools were selected from a certain city. The inclusion criteria for subjects were: 1. Current students in the first grade of junior high school; 2. No organic diseases of the cardiovascular or bone and joint systems; 3. Parents signed a written informed consent form, and the students themselves agreed. Exclusion criteria: 1. Received systematic physical training in the past 6 months; 2. Contraindicated use of smartphones or wearable devices; 3. Cognitive impairment affects the understanding of instructions. Finally, 1286 people were included (647 in the experimental group and 639 in the control group).

The experimental group implemented AI personalized teaching intervention: each physical education class was 40 minutes, including 5 minutes of warm-up, 30 minutes of AI-generated main training, and 5 minutes of relaxation and organization; teachers made collaborative adjustments based on the push intervention package; daily training data was uploaded to the private cloud in real time. The control group follows the current physical education curriculum standards. The content and intensity are regulated by teachers based on experience, and no smart devices or algorithm feedback are introduced.

All tests are performed by 6 third-party sports experts and uniformly trained. The baseline test was completed within 7 days before the intervention, covering 6 key physical fitness indicators (standing long jump, 4×15m return run, 1000m/800m run, pull-ups/sit-ups, seated forward flexion, 30-second double jump); the post-test was completed within 48 hours after the 12-week intervention, and the venue, equipment, test period, and tester allocation remained the same. This study was approved by the Ethics Committee of Beibu Gulf University, and was performed in accordance with the principles of the Declaration of Helsinki. All eligible participants signed an informed consent form.

B. ASSESSMENT OF IMPROVEMENT IN KEY PHYSICAL ABILITIES

This section uses the standardized pre-post-test difference method to quantify the net improvement effect of 6 key physical fitness characteristics, which is performed by uniformly trained third-party physical education researchers to eliminate evaluator bias. Each indicator has a perfect score of 100, and the extent of improvement is evaluated based on the improvement in scores. SD (Standard Deviation)

Explosive power: represented by changes in standing long jump performance. The test is conducted on a flat plastic ground. The subject is barefoot and stands with feet parallel behind the take-off line. After swinging the arms, both feet take off at the same time. After landing, the body is not allowed to sit back or support the ground with hands. Measure the vertical distance from the rear edge of the take-off line to the rear edge of the nearest landing point, accurate to 0.5 cm. Each person tests 3 times and takes the best value. Sensitivity: evaluated using the time difference of the 4×15 meter return run. The test is conducted on a 15-meter straight track, with 30 cm high and 5 cm wide sign barrels set up at both ends; the subject stands behind the starting line, sprints to 15 meters and returns around the sign barrel after hearing the "Run" command, and repeats the return run 4 times; the timer uses an electronic timer and stops the timing as soon as the trunk reaches the finish line; each person is tested twice, with an interval of 3 minutes, and the better value is taken. The amplitude of improvement is defined as the pretest time minus the posttest time, with positive values indicating increased sensitivity. Endurance: measured by changes in boys' 1,000-meter run and girls' 800-meter run. The test is conducted on a standard 400-meter plastic track, with a group of 5-8 people starting from a standing position; the timekeeper uses two people to synchronize timing at the finish line, and takes the average of the two people; the results are accurate to 0.1 s. Core Stability: Pull-ups for boys and sit-ups for 1 minute for girls. Pull-ups require both hands to hold the horizontal bar, the body is still and hanging as the starting point, and the lower jaw passes the bar to complete one time, and the body is not allowed to swing to use force; sit-ups require bending the knees at 90°, fixing the soles of the feet, crossing the arms against the chest, and touching the elbows to the knees to be effective; each count is counted as one effective completion time. The improvement is the number of post-tests minus the number of pre-tests. Flexibility: Measured using seated forward flexion. The subject sat in front of the tester with his legs straight, the soles of his feet against the vertical baffle, his hands together and slowly pushed the cursor forward; the knee joints were required to keep straight and the head to droop naturally; the cursor displacement was recorded by the electronic sensor; each person was tested twice, and the maximum value was taken. The improvement range was the post-test value minus the pre-test value. Coordination: Evaluate the number of times you can jump rope with double swings for 30 seconds. A uniformly distributed steel wire rope is used, and the ground is an indoor wooden floor; it is required to jump with both feet together, and the rope body is wrapped around the body twice each time; the counter is specially trained, and only counts two complete circles with both wrists and a single movement of the feet off the ground; the test is performed once and lasts for 30 seconds. The improvement range is the number of post-tests minus the number of pre-tests, reflecting the coupling ability of the rope-swinging rhythm of the upper limbs and the jumping timing of the lower limbs. Key physical fitness improvements after the 12-week intervention are shown in Figure 4.

The data in Figure 4 visually shows that after 12 weeks of intervention, the AI-driven personalized teaching model has improved in six key physical fitness indicators compared with the control group. The average score of the experimental group increased by 12.3 points (percentage system). Specifically, the experimental group increased 8.2±2.1 points in Explosiveness, compared with 3.1±1.9 points in the control group; the score in Agility increased by 10.5±1.8 points, which was 1.5±0.9 points higher than that in the control group; the score in Endurance increased by 12.6±2.2 points, which was overall 4.8±2.8 points higher than that in the control group; Core Stability (Core) Stability) increased by 12.8±1.3 points, compared with only 1.3±1.1 points in the control group; flexibility increased by 13.1±1.0 points, which was better than the 1.2±0.5 points in the control group; coordination increased by 16.4±1.1 points, which was better than 2.2±1.5 points in the control group. These data not only prove the effectiveness of the AI model but also reveal its huge potential in improving students' comprehensive sports ability.

C. INDIVIDUAL ADAPTABILITY ASSESSMENT

In order to quantify the accuracy of the model's response to individual dynamic needs, this study constructed an adaptability index, which was calculated in single-session units. Finally, the 12-week median was used as the individual-level evaluation index to avoid interference from extreme values. Fifty students from the experimental group were randomly selected for 12 weeks of continuous follow-up. The dynamic evolution trend of individual adaptability index is shown in Figure 5.

Figure 5 shows the dynamic evolution trend of the individual adaptability index of the 50 students in the experimental group during the 12-week intervention period. Each polyline represents a student, and the overall trend is upward. The average value in the first week was 0.732, and by the 12th week, the average value increased to 0.901, with an increase of 0.169, indicating that the system gradually improved the accuracy of personalized control over time. It is worth noting that the individual adaptability index of some students was low (0.61-0.65 range) from 1 to 3 weeks, but most of them improved as the number of training weeks increased. By 12 weeks, only 5 students had an individual adaptability index lower than 0.8, reflecting the system's continuous optimization ability for "difficult to adapt individuals".

D. ASSESSMENT OF CHANGES IN TRAINING INJURY RISK

This study used training load volatility as a core proxy for injury risk. The assessment is based on individuals, and the coefficient of variation is calculated based on 12 weeks of longitudinal TRIMP data, reflecting the stability of the load arrangement.

The data source is heart rate and exercise duration data continuously collected by smart bracelets worn by students in the experimental group. After denoising through the preprocessing process, the TRIMP value of each class is calculated. The TRIMP value of a single week is the sum of the TRIMP of all valid physical education classes in that week. Missing classes are interpolated with the mean of the student's remaining classes that week.

The weekly TRIMP sequence is standardized: for each student, the mean and standard deviation of the 12- week TRIMP are calculated, and then the weekly fluctuation coefficient is obtained. The final individual injury risk index is defined as the arithmetic mean of the 12-week fluctuation coefficient. The higher it is, the more likely it is to be injured. The weekly fluctuation coefficients of the two groups are shown in Figure 6.

Figure 6 shows the distribution of weekly training load fluctuation coefficients for students in the experimental group and the control group during the 12-week intervention period. The higher the value, the more severe the change in load between weeks is, and the more likely it is to cause sports injuries. From the data of the experimental group in Figure 6(a), it can be seen that the fluctuation

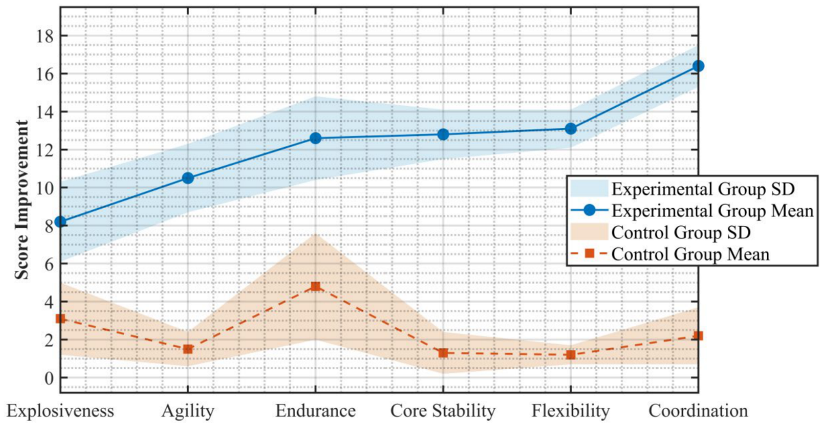

FIGURE 4. Key Physical Fitness Improvements after 12 Weeks of Intervention

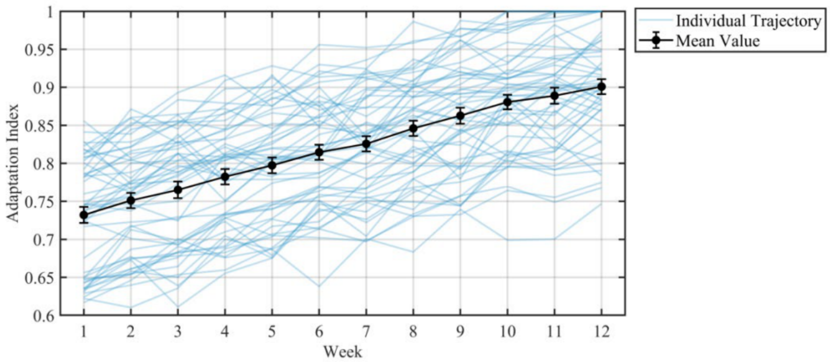

FIGURE 5. Dynamic Evolution Trend of Individual Adaptability Index

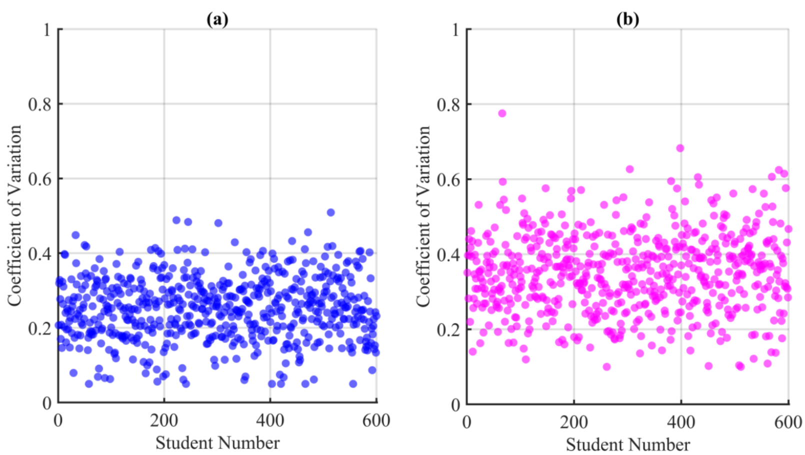

FIGURE 6. Weekly Fluctuation Coefficient. (a) Weekly Fluctuation Coefficient of Experimental Group; (b) Weekly Fluctuation Coefficient of the Control Group

coefficient is generally concentrated in the lower range, with most samples falling between 0.1-0.4, while in the control group of Figure 6(b) it has increased significantly, with a large number of individuals exceeding 0.4. Overall observation shows that the average fluctuation coefficient of the experimental group is lower than that of the control group, indicating that the method in this paper achieves precise and stable control of the load.

E. EVALUATION OF EFFICIENCY IN ACHIEVING TEACHING GOALS

This section focuses on the efficiency of quantitative teaching intervention in promoting students to reach the excellent level ($\geq$90 points) per unit time, to avoid focusing only on

TABLE 1. Standard Deviation of Goal Achievement Efficiency of Experimental Group

Week	Explosiveness	Agility	Endurance	Core Stability	Flexibility	Coordination
1	0.42	0.31	0.47	0.28	0.21	0.17
2	0.51	0.39	0.58	0.33	0.26	0.22
3	0.57	0.43	0.62	0.35	0.29	0.25
4	0.61	0.46	0.65	0.37	0.31	0.27
5	0.63	0.48	0.67	0.38	0.32	0.28
6	0.65	0.49	0.68	0.39	0.33	0.29
7	0.64	0.47	0.66	0.38	0.32	0.28
8	0.66	0.50	0.69	0.40	0.34	0.30
9	0.68	0.52	0.71	0.41	0.35	0.31
10	0.69	0.53	0.72	0.42	0.36	0.32
11	0.71	0.55	0.74	0.43	0.37	0.33
12	0.73	0.56	0.75	0.44	0.38	0.34

TABLE 2. Standard Deviation of Goal Achievement Efficiency in the Control Group

Week	Explosiveness	Agility	Endurance	Core Stability	Flexibility	Coordination
1	0.68	0.54	0.71	0.49	0.38	0.32
2	0.87	0.69	0.93	0.61	0.50	0.42
3	1.05	0.84	1.12	0.75	0.61	0.51
4	1.18	0.94	1.26	0.85	0.69	0.58
5	1.27	1.01	1.35	0.92	0.74	0.63
6	1.34	1.07	1.42	0.97	0.78	0.67
7	1.39	1.11	1.47	1.01	0.81	0.70
8	1.43	1.14	1.51	1.04	0.84	0.72
9	1.46	1.17	1.54	1.06	0.86	0.74
10	1.49	1.19	1.57	1.08	0.88	0.75
11	1.52	1.21	1.60	1.10	0.89	0.77
12	1.55	1.23	1.63	1.12	0.91	0.79

average changes and ignoring distribution migration.

Calculate the achievement efficiency in single items: for each physical ability, count the number of people who have reached $\geq$90 points before the experiment and the number of people who have reached $\geq$90 points after the intervention. The total sample size is the number of effective subjects who completed the pre- and post-tests. Standard compliance efficiency is defined as the average weekly proportion of new people who meet the standard. This indicator strips away base effects and allows comparison of advancement rates across projects. The goal achievement efficiency is shown in Figure 7.

Figure 7 shows the target achievement efficiency of the six key physical characteristics of the experimental group and the control group during the 12-week intervention period, that is, the average proportion of new students promoted from non-excellent level (<90 points) to excellent level ($\geq$90 points) every week. As can be seen from Figure 7(a), the efficiency of various physical abilities in the experimental group showed a steady upward trend. At 12 weeks, the explosive power reached 39.8%, the endurance reached 42.6%, and the coordination reached 15.7%. Among them, endurance and explosive power improved the fastest; while in Figure 7(b), although the control group also showed an increasing trend, the overall values were significantly lower. At 12 weeks, the explosive power was only 18%, endurance was 21.6%, and coordination was 6%. This data difference stems from the underlying mechanism of the dynamic adaptive AI teaching model constructed in this article. The double-loop reinforcement learning framework can dynamically adjust training intensity and action sequences based on students' real-time physiological and kinematic feedback, and accurately match high-contribution actions. At the same time, the teacher's collaborative intervention interface automatically pushes structured intervention packages for individuals with stagnant learning, greatly reducing ineffective repetitive training. The standard deviation of the goal achievement efficiency of the experimental group and the control group is shown in Tables 1 and 2.

Tables 1 and 2 respectively show the standard deviation changes in the achievement efficiency of each key physical fitness indicator goal between the experimental group and the control group during the 12-week intervention period. The standard deviation of each indicator in the experimental group remained at a low level overall, with explosive power steadily increasing from 0.42 in the first week to 0.73 in the 12th week, and coordination increasing from 0.17 to 0.34; while the standard deviation of the control group was higher, such as explosive power rising from 0.68 to 1.55, endurance rising from 0.71 to 1.63, and core stability rising from 0.49 to 1.12. This shows that the individual differences of students in the experimental group have converged and their teaching responses have been stable under AI personalized intervention, which proves that the AI model has significantly improved the homogeneity and predictability of the teaching process.

F. STUDENTS PARTICIPATE IN CONTINUOUS ASSESSMENT

This section objectively quantifies the long-term participation status of students from the two dimensions of behavioral compliance and independent investment to avoid the social desirability bias caused by relying on subjective questionnaires. Data collection relies on dual mechanisms of system logs and manual verification to ensure timing integrity and behavioral authenticity.

Absence rate: Based on the classroom sign-in record, students in the experimental group need to complete face recognition sign-in on the APP (Application) interface of the teacher's Pad, and the system automatically marks the time stamp; in the control group, the physical education teacher enters the roll call on paper and enters it into the spreadsheet on the same day; the two types of data are automatically synchronized to the central database at 22:00 every day. Absence is defined as incomplete sign-in and no valid sick leave/personal leave certificate; lateness for more than 5 minutes is recorded as half absence, and lateness for more than 15 minutes is recorded as full absence. The absenteeism rate is calculated as the cumulative number of absences for each student within 12 weeks divided by the total number of theoretically attended classes, then multiplied by 100%. During the data cleaning phase, dates that were uniformly suspended due to school-wide activities were eliminated to ensure consistency in the denominator. Independent practice rate: objectively captured through the APP background behavior log, defined as the frequency of

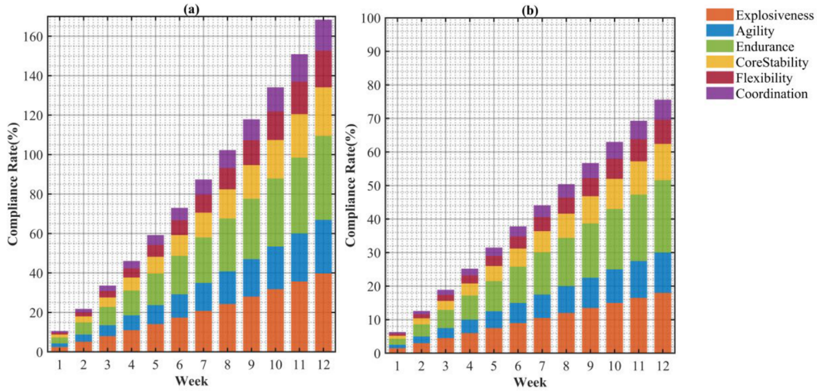

FIGURE 7. Goal Achievement Efficiency. (a) Experimental Group Goal Achievement Efficiency; (b) Goal Achievement Efficiency of the Control Group

effective additional practice behavior with teaching significance. The specific determination process is as follows: 1. Students start the "autonomous training" module of the APP during non-physical education periods; 2. The system detects movements in real time; 3. Only when the confidence of movement recognition is high and a complete movement cycle is detected within 10 consecutive seconds, it is counted as a valid additional training session; 4. The duration of a single session must be $\geq$ 60 seconds, and the session interval is > 10 minutes before it can be counted repeatedly. The number of effective additional training sessions is counted every week. If there are $\geq$ 2 times, the week is marked as "the week of independent additional training to achieve the standard"; the independent additional training rate is the proportion of weeks that meet the standard within 12 weeks. In order to prevent fraud, the system sets up anti-counterfeiting mechanisms such as scene verification, action constraints, and geographical location. The backend logs are encrypted and stored, and 5% of the video clips are sampled by independent auditors every week to review the authenticity of the actions. The absenteeism rate and independent training rate of students in the experimental group are shown in Figure 8.

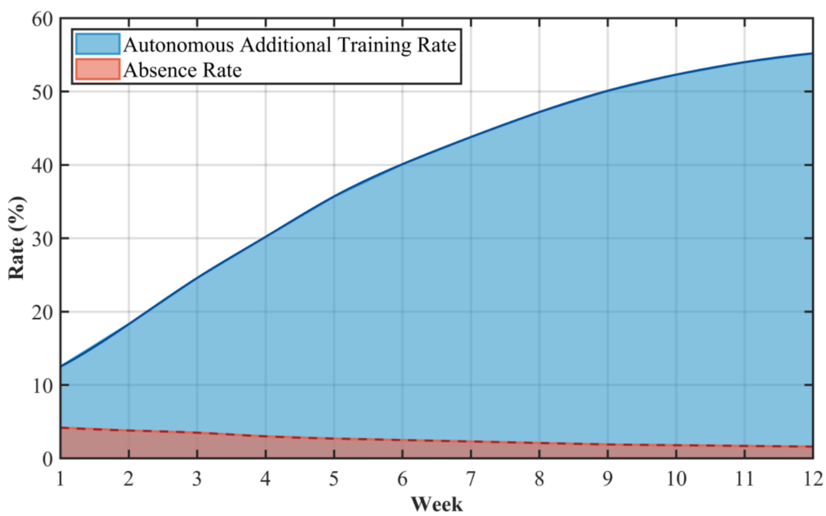

FIGURE 8. Absence Rate and Independent Practice Rate of Students in the Experimental Group

Figure 8 shows the dynamic trend of the absenteeism rate and independent practice rate of students in the experimental group during the 12-week intervention period. The data reflects that personalized teaching significantly improves students' willingness to participate and behavioral investment. The absenteeism rate continued to decrease from 4.2% in the first week to 1.6% in the 12th week, showing a stable convergence trend; at the same time, the independent training rate steadily climbed from 12.5% in the first week to 55.2% in the 12th week, indicating that as the degree of personalization of teaching increases and students' physical fitness benefits appear, absenteeism decreases and the willingness to actively invest increases, forming a virtuous circle.

IV. CONCLUSION

To address the contradiction between rigid physical education curricula and the dynamic individual differences of students, this study proposes an artificial intelligence-driven personalized teaching model that optimizes educational outcomes through a precision-tailored approach modeled. By integrating computer vision, wearable sensors and expert knowledge graphs, a closed-loop system is built from real-time action analysis, dynamic student portraits to personalized training plan generation. Experimental verification shows that the average score on key physical fitness indicators is 12.3 points (percentage system), and the average individual adaptability index is increased from 0.732 to 0.901.

The proposed personalized teaching framework achieves continuous perception and response to dynamic student characteristics, effectively promoting the precise enhancement of physical attributes through a technical path that mirrors the high-resolution sensing and adaptive feedback loops found in intelligent manufacturing. By integrating these cross-disciplinary principles, the model provides a replicable practical basis for implementing smart physical education.

AUTHOR CONTRIBUTIONS

Conceptualization –Xiaoyan Hu and Minghuan Tang; methodology – Xiaoyan Hu and Minghuan Tang; investigation – Xiaoyan Hu and Minghuan Tang; writing-original draft preparation – Xiaoyan Hu and Minghuan Tang. All authors have read and agreed to the published version of the manuscript.

CONFLICTS OF INTEREST

The authors declare no conflict of interest.

FUNDING

This research was supported by,

2023 National Philosophy and Social Science Fund Project: Research on Effective Utilization of Red Sports and Cultural Resources in the Left and Right River Revolutionary Old Areas (23CTY016).

Ethics Approval and Consent to Participate This study was approved by the Ethics Committee of Beibu Gulf University, and was performed in accordance with the principles of the Declaration of Helsinki. All eligible participants signed an informed consent form.

ACKNOWLEDGEMENTS

Not applicable.

REFERENCES

[1] Y. Na, “Innovative Teaching Models of Physical Education and Health in Junior Middle Schools under the Integration of Information Technology,” Journal of International Education and Science Studies Vol, vol. 2, no. 9, pp. 188-191, 2025, doi: 10.62639/sspjiess32.20250209.

[2] A. Ascione, “Physical education and artificial intelligence at school,” Journal of inclusive methodology and technology in learning and teaching, vol. 4, no. 1, pp. 1-15, 2024, doi: 10.32043/jimtlt.v4i1.141.

[3] F. Pratiwi and S. D. Loviani, “Leveraging Artificial Intelligence to Enhance Physical Education in Elementary Schools: A Systematic Review and Future Directions,” Indonesian Journal of Sport Management, vol. 4, no. 3, pp. 335-351, 2024, doi: 10.31949/ijsm.v4i3.11012.

[4] W. Forero-Corba and F. N. Bennasar, “Techniques and applications of Machine Learning and Artificial Intelligence in education: a systematic review,” RIED-Revista Iberoamericana de Educación a Distancia, vol. 27, no. 1, pp. 1-35, 2024, doi: 10.5944/ried.27.1.37491.

[5] V. V. Ramires, P. C. D. Santos, V. C. B. Filho, A. D. S. Bandeira, M. C. M. Tenório, Camargo EMd, et al., “Physical education for health among school-aged children and adolescents: a scoping review of reviews,” Journal of Physical Activity and Health, vol. 20, no. 7, pp. 586-599, 2023, doi: 10.1123/jpah.2022-0395.

[6] A. Garcia-Hermoso, J. F. Lopez-Gil, and Y. Ezzatvar, “Tracking of physical activity and sport from childhood and adolescence to adulthood: a systematic review and meta-analysis,” Translational Pediatrics, vol. 14, no. 6, pp. 1117-1128, 2025, doi: 10.21037/tp-2025-89.

[7] L. Wei and S. J. Wang, “Motion tracking of daily living and physical activities in health care: Systematic review from designers’ perspective,” JMIR mHealth and uHealth, vol. 12, no. 1, Art. no. e46282, 2024, doi: 10.2196/46282.

[8] S. Li, C. Wang, and Y. Wang, “Fuzzy evaluation model for physical education teaching methods in colleges and universities using artificial intelligence,” Scientific Reports, vol. 14, no. 1, pp. 4788-4810, 2024, doi: 10.1038/s41598-024-53177-y.

[9] A. Cudicio, S. Sangalli, L. Lucaccioni, and A. Borgogni, “Artificial intelligence in personalizing physical education: a two-year study,” Giornale Italiano di Educazione alla Salute, Sport e Didattica Inclusiva, vol. 8, no. 2, pp. 1-14, 2024, doi: 10.32043/gsd.v8i2.1119.

[10] Y. Xin and H. Bu, “Artificial Intelligence Helps Youth Sports Education: The Road to the Integration of Personalization and Precision,” Leisure Sports and Health, vol. 4, no. 3, pp. 80-85, 2024, doi: 10.35534/lsh.0403014.

[11] M. Cao, “An Advanced Apriori Algorithm Technology to Enhance Sports Data Mining,” Information Resources Management Journal (IRMJ), vol. 37, no. 1, pp. 1-18, 2024, doi: 10.4018/IRMJ.361709.

[12] G. Li and J. Liu, “Improving physical education through innovative multimedia learning platform and datadriven instruction,” Soft Computing, vol. 28, no. 2, pp. 1567-1584, 2024, doi: 10.1007/s00500-023-09436-7.

[13] Y. Tian, “Research on Physical Education Teaching Improvement Strategies and Algorithms Based on Big Data Analysis,” Scalable Computing: Practice and Experience, vol. 26, no. 2, pp. 993-1003, 2025, doi: 10.12694/scpe.v26i2.3938.

[14] C. Mou and Q. Dong, “The data-driven intelligent system for physical education utilizing data mining and virtual simulation technologies,” Journal of Computational Methods in Sciences and Engineering, vol. 25, no. 2, pp. 1617-1629, 2025, doi: 10.1177/14727978241302163.

[15] Q. Huang and L. Li, “Using Deep Learning Algorithms to Generate Personalized Training Plans for Taekwondo Competitions of Physical Education Majors,” World Scientific Research Journal, vol. 10, no. 7, pp. 65-74, 2024, doi: 10.6911/WSRJ.202407_10(7).0007.

[16] Q. Li, P. M. Kumar, and M. Alazab, “IoT-assisted physical education training network virtualization and resource management using a deep reinforcement learning system,” Complex & Intelligent Systems, vol. 8, no. 2, pp. 1229-1242, 2022, doi: 10.1007/s40747-021-00584-7.

[17] J. Chen, G. Zhou, and Y. Zhong, “A personalized recommendation system for teaching resources in sports using fuzzy C-means clustering technique,” Soft Computing-A Fusion of Foundations, Methodologies & Applications, vol. 28, no. 1, pp. 703-724, 2024, doi: 10.1007/s00500-023-09421-0.

[18] H. Die and L. Lianhong, “Research on the optimization of the physical education teaching mode based on cluster analysis under the background of big data,” Scientific Programming, vol. 2022, no. 1, pp. 6340526-6340542, 2022, doi: 10.1155/2022/1293676.

[19] J. W. Kim, J. Y. Choi, E. J. Ha, and J. H. Choi, “Human pose estimation using mediapipe pose and optimization method based on a humanoid model,” Applied sciences, vol. 13, no. 4, pp. 2700-2712, 2023, doi: 10.3390/app13042700.

[20] S. Kale, N. Kulkarni, S. Kumbhkarn, A. Khuspe, and S. Kharde, “Posture detection and comparison of different physical exercises based on deep learning using media pipe, opencv,” International Journal of Scientific Research in Engineering and Management, vol. 7, no. 04, pp. 1-29, 2023, [Online]. Available: https://ijsrem.com/download/posture-detection-and

-comparison-of-different-physical-exercises-based-on-deep-learning-usingmedia-pipe-opencv/.

[21] Y. Kwon and D. Kim, "Real-time workout posture correction using OpenCV and MediaPipe," The Journal of Korean Institute of Information Technology, vol. 20, no. 1, pp. 199-208, 2022, doi: 10.14801/jkiit.2022.20.1.199.

[22] D. Suescun-Diaz, G. Ule-Duque, and L. E. Cardoso-Paez, "Butterworth filter to reduce reactivity fluctuations," Karbala International Journal of Modern Science, vol. 10, no. 1, pp. 8-16, 2024, doi: 10.33640/2405-609X.3342.

[23] M. Schmid, D. Rath, and U. Diebold, "Why and how Savitzky-Golay filters should be replaced," ACS Measurement Science Au, vol. 2, no. 2, pp. 185-196, 2022, doi: 10.1021/acsmeasuresciau.1c00054.

[24] M. H. Abdillah, "Implementation of Forgy Initialization and K-Means++ Algorithms in the K-Means Clustering Method for Sales Data Analysis of Dazzle Store," Telematika: Jurnal Telematika dan Teknologi Informasi, vol. 22, no. 2, pp. 149-156, 2025, doi: 10.31315/telematika.v22i2.14468.

[25] R. Aliguliyev and S. F. Tahirzada, "PERFORMANCE COMPARISON OF K-MEANS, PARALLEL K-MEANS AND K-MEANS++," Reliability: Theory & Applications, pp. 20(SI 7 (83)):169-176, 2025, [Online]. Available: https://cyberleninka.ru/article/n/performance-comparison-of-k-means-parallel-k-means-and-k-means.

[26] G. R. Corominas, M. J. Blesa, and C. Blum, "Accelerating the k-means++ algorithm by using geometric information," IEEE access, vol. 13, no. 1, pp. 67693-67717, 2025, doi: 10.1109/ACCESS.2025.3561293.

[27] M. Beraha and M. Pegoraro, "Wasserstein principal component analysis for circular measures," Statistics and Computing, vol. 34, no. 5, pp. 171-188, 2024, doi: 10.1007/s11222-024-10473-x.

[28] P. Zoubouloglou, E. Garcia-Portugues, and J. S. Marron, "Scaled torus principal component analysis," Journal of Computational and Graphical Statistics, vol. 32, no. 3, pp. 1024-1035, 2023, doi: 10.1080/10618600.2022.2119985.

[29] T. Sablatzky, "The delphi method," Hypothesis: Research Journal for Health Information Professionals, vol. 34, no. 1, pp. 1-6, 2022, doi: https://doi.org/10.18060/26224.

[30] X. Yang, Z. Xu, and J. Xu, "Large-scale group Delphi method with heterogeneous decision information and dynamic weights," Expert Systems with Applications, vol. 213, no. 1, pp. 118782-118794, 2023, doi: 10.1016/j.eswa.2022.118782.

[31] Z. H. Chao, Y. Y. Long, L. Yi, and L. Min, "Deep Q Learning-Enabled Training and Health Monitoring of Basketball Players Using IoT Integrated Multidisciplinary Techniques," Mobile Networks and Applications, vol. 1, no. 1, pp. 1-16, 2024, doi: 10.1007/s11036-024-02376-y.

[32] H. Xu, B. Lin, and L. Liu, "Design of intelligent optimization of sports strategy and training decision support system based on deep reinforcement learning," Discover Artificial Intelligence, vol. 5, no. 1, pp. 219-226, 2025, doi: 10.1007/s44163-025-00473-9.

[33] W. Han, M. Hao, Y. Yuan, and P. Liu, "Fusion enhancement of yolov5 and copula bayesian classifier for hand gesture recognition in smart sports venues," IEEE Access, vol. 12, no. 1, pp. 67005-67012, 2024, doi: 10.1109/access.2024.3398142.

[34] K. Zhao, "Enhancing the Performance and Accuracy in Real-Time Football and Player Detection Using Upgraded YOLOv5 Architecture," International Journal of Computational Intelligence Systems, vol. 17, no. 1, pp. 163-178, 2024, doi: 10.1007/s44196-024-00565-x.

[35] D. P. Putro, I. Gunawan, and P. E. Suryani, "Software Push Notification Disposisi Persuratan Berbasis Website Menggunakan Firebase Cloud Messaging," Journal of Information Technology Ampera, vol. 3, no. 3, pp. 370-381, 2022, doi: 10.51519/journalita.volume3.isssue3.year2022.page370-381.